

## Stochastic resonance in vertical cavity surface emitting lasers

Sylvain Barbay,<sup>1</sup> Giovanni Giacomelli,<sup>1,2,\*</sup> and Francesco Marin<sup>2,3</sup>

<sup>1</sup>*Istituto Nazionale di Ottica, Largo Enrico Fermi 6, 50125 Firenze, Italy*

<sup>2</sup>*INFM, unità di Firenze, Firenze, Italy*

<sup>3</sup>*Dipartimento di Fisica, Università di Firenze, and Laboratorio Europeo di Spettroscopia Nonlineare (LENS),*

*Largo Enrico Fermi 2, 50125 Firenze, Italy*

(Received 7 May 1999)

We report a detailed experimental investigation of stochastic resonance (SR) in the polarized emission of a pump-modulated vertical cavity surface emitting laser. We characterize SR in the time and frequency domains, with a quantitative agreement with existing theories. We further report a statistical analysis of SR in terms of residence-time probability distributions exhibiting alternative features which are fully explained here. By using an accurate choice of the indicator, we are also able to give clear evidence of *bona fide* resonance.

PACS number(s): 42.65.Sf, 42.55.Sa, 42.50.-p

### I. INTRODUCTION

The phenomenon known as stochastic resonance (SR) has been the subject of intensive investigations in recent years. The term describes a particular behavior of the response of a bistable system when a weak coherent signal is superimposed to stochastic fluctuations as an input. One commonly expects that an increase of the noise level leads to a deterioration of the performance. In such systems, however, the noise can induce synchronized jumps between the two stable states, producing a strong output signal. Hence, the response of the bistable system shows a resonancelike behavior versus the input noise level, which is the main signature of SR.

This idea was first introduced in 1981 by Benzi *et al.* [1,2] and by Nicolis and Nicolis [3] to explain the periodicity of the ice ages in the quaternary climate. There, the small periodic input is represented by the modulation of the earth's orbital eccentricity, while the fluctuations are due to the year-to-year variations of the solar activity. The phenomenon was later reproduced by Fauve and Heslot [4] using an electronic circuit based on a Schmitt trigger.

The great increase of interest in SR originates from the first experimental observation in a bistable ring laser performed in 1988 by McNamara *et al.* [5], who found a resonance in the signal-to-noise ratio as a function of the input noise strength. After this work, SR was the subject of wide investigations mainly based on theoretical studies [6] and analog simulations [7–9], devoted to a better understanding of the various aspects of the phenomenon. The amount of work is considerably large and we may refer to the very exhaustive recent review by Gammaitoni *et al.* [10]. At the same time, SR has been observed in a large variety of systems studied in different fields, from neurophysiology (in the neuronal processes), to solid-state physics [tunnel diodes, superconducting quantum interference device (SQUIDs)], which confirms its wide interdisciplinary interest (see, e.g., [11]). After the work described in [5], two other groups recently observed SR in laser systems, namely, in a CO<sub>2</sub> laser with intracavity absorber [12] and in a two-section semicon-

ductor distributed-feedback laser [13]. In both experiments, the signature of SR is the maximum of the output signal, when a Gaussian noise of variable strength is superimposed onto a small modulation in the pump current. However, experimental work far from permits a complete and satisfactory comparison with the rich amount of theoretical results. Investigation of the most intriguing aspects of SR is mainly limited to a comparison between analytical calculations and numerical and analog simulations.

We discuss quite a different situation in our preliminary work [14], where we also report the experimental evidence of SR considered as *bona fide* resonance, i.e., as a function of the input modulation frequency. The system studied in [14] is based on a vertical cavity surface emitting laser (VCSEL) whose emission intensity is observed, after polarization selection, when a sinusoidal signal and a Gaussian noise are superimposed onto the injection current. With respect to previous experimental works our system has the advantages of allowing one to change the input parameters (modulation frequency and amplitude, noise intensity and bandwidth) over a large range. The system intrinsic parameters, i.e., the shape of the quasipotential and the characteristic residence times, can also be changed acting on the injection current or selecting the laser sample. These features, together with the high stability and reproducibility, allow an unprecedented comparison with theoretical work; for example, the study of SR as a function of modulation frequency and a complete characterization of the SR by means of probability distributions are reported in [14].

In the present work, we present a detailed description of the investigation of SR with VCSELs. In Sec. II the experimental apparatus is described. In Section III we report an analysis of the polarization dynamics of VCSELs. A complete set of parameter calibrations allows a direct comparison with the theory. In Sec. IV we analyze the temporal evolution of the laser-polarized intensity versus the input noise level. In Sec. V, we perform an analysis of SR in terms of residence-time probability distributions in the two states. With this technique, we can also show a *bona fide* resonance.

A critical point for the use of the probability distributions in the description of the dynamics is the choice of the indicator for the SR. The indicators we have used in [14], i.e.,

\*Author to whom correspondence should be addressed. FAX: +39-055-2337755. Electronic address: gianni@ino.it

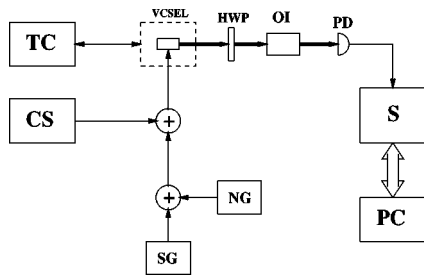


FIG. 1. Experimental setup. CS, current source; TC, temperature controller; SG, signal generator; NG, noise generator; HWP, half wave plate; OI, optical isolator; PD, photodiode; S, digital scope.

the area of the peaks after background subtraction, are discussed here in detail.

## II. EXPERIMENTAL SETUP

We employ a commercial, quantum-well VCSEL, lasing at 840 nm with distributed Bragg reflectors. The emission window has a diameter of about  $15 \mu\text{m}$ ; the current confinement and isolation are provided by proton implantation. The laser is thermally stabilized (better than 1 mK) and the pump current is carefully controlled with a noise of about  $70 \text{ pA}/\sqrt{\text{Hz}}$  in the range 1 kHz to 3 MHz. The overall stability allows long time measurements, even in the presence of critical behaviors. An optical isolator prevents optical feedback effects, while an half-wave plate before the input polarizer permits one to select a linear polarization. The laser intensity is monitored by a fast avalanche detector (bandwidth greater than 1 GHz) whose signal is acquired by a digital scope (1 GHz bandwidth). The signals from a 10 MHz bandwidth white noise generator and a sinusoidal oscillator are summed and coupled into the laser input current, after a 6 dB attenuation.

The experimental setup is shown in Fig. 1.

## III. BISTABLE BEHAVIOR OF THE VCSEL

The emission of VCSELs is characterized by strong polarization fluctuations, due to their almost-cylindrical symmetry. Small anisotropies lead to a selection of two perpendicular polarization directions (along the  $[1\bar{1}0]$  and  $[110]$  axes of the semiconductor crystal), although laser light can be emitted on both polarizations, depending on the laser structure and on the pump current. As a consequence, the polarization noise is often much larger than the intensity noise [15]. Furthermore, VCSELs show a complicated spatial emission in the transverse plane due to the large Fresnel number of the laser cavity. A phenomenon often observed, and crucial to the present work, is the switching of transverse modes from one polarization direction to the other, which occurs for some particular values of the pump current [16,17].

We have observed previously [18] that the switch is not abrupt, but we should rather speak of a switching region of the pump current. In this region, the laser intensity in one polarization displays frequent jumps between two levels, corresponding to different configurations of the laser emission. This effect clearly appears while observing the histograms of the polarized intensity fluctuations: while a normal

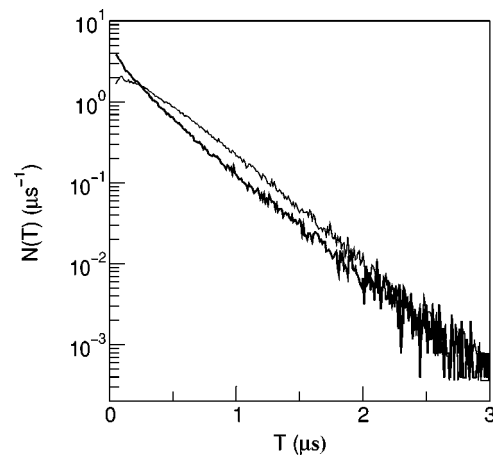


FIG. 2. Normalized histograms  $N(T)$  of the residence times  $T$  in the upper (thin line) and lower (thick line) state for  $\Delta V/D=0.174$ .

behavior is characterized by a Gaussian distribution, in the switching region the histogram has a distorted shape and exhibits two peaks corresponding to the above-mentioned levels.

We notice that this phenomenon was observed only by selecting the polarization of the laser before the detection. Indeed, no effect could be noticed in the total intensity. This means that the fluctuations in the two polarizations are strongly anticorrelated, and consequently cancel out upon detection of the total emission. An anticorrelation up to  $C \approx -0.997$  was actually directly measured [19] ( $C$  being the normalized cross correlation of the two polarization intensities ranging from 1 for perfect correlation to  $-1$  for perfect anticorrelation).

Once the two levels involved in the dynamics are defined, we investigate the statistics of the residence times in the states, between two polarization jumps, finding an exponential distribution typical of a van't Hoff–Arrhenius law [20–22]. In the present work the characteristic time of the exponential function (Kramers time [23]) is of the order of  $1 \mu\text{s}$ . Figure 2 shows an example of the residence-time histograms for both states. We can reproduce quite well the observed behavior by using a simple Langevin model [19]. In this model, the temporal evolution of the intensity  $q$  in one polarization is determined by a quasipotential  $V(q)$  and a stochastic term  $F(t)$ ,

$$\dot{q} = -\frac{\partial V(q)}{\partial q} + F(t). \quad (1)$$

In the switching region,  $V(q)$  has a two-well shape, with the abscissa of the minima corresponding to the two intensity levels (upper and lower). Jumps between the two wells are driven by the Langevin term. In such a system, the probability distribution  $P(q)$  is given in general by (see, e.g., [24,25])

$$P(q) = P_0 \exp\left(-\frac{V(q)}{D}\right), \quad (2)$$

where  $P_0$  is a normalization constant and  $D$  is the diffusion coefficient defined by

$$\langle F(t')F(t'') \rangle = 2D \delta(t' - t''). \quad (3)$$

Inverting Eq. (2), we deduced the phenomenological quasipotentials from the experimental histograms of the polarized intensity for different values of the pump current. An important result of [19] is that the dynamics of the system and the Kramers times can be accurately reproduced for the whole range of current and for both upper and lower levels, using only one single value of  $D$ : the jumps are driven by noise terms which do not change significantly within the switching region. Another important observation inferred from the model, and in particular from the shape of the quasipotentials, is that the polarization flip would have indeed an hysteretic dependence on the pump current, but this feature is masked by the noise-driven jumps.

For a more realistic model of the laser behavior, one must take into account different transverse modes, as suggested by a spatially selective analysis of the intensity fluctuations [26]. The results obtained using the model introduced in Ref. [27], together with the comparison with the experiments, are reported elsewhere [28]. However, a complete understanding of the VCSEL behavior is still the object of extensive work (see [29] for a review and [30] for recent developments) and it is not the aim of this paper.

The particular features of the VCSELs behavior described up to now are rather general. In our work we have used VCSEL samples with a structure which is different with respect to the one of our above-mentioned papers. Here, the spatial profile of the emission is rather complex and the polarization jumps of the intensity are found for different current values, corresponding to transitions between various emission patterns. While a satisfactory microscopic model of the laser behavior is now even more difficult to develop, we stress that the evolution of the polarized intensity can again be locally described with the same Langevin model. Moreover, the characteristic Kramers times can greatly vary for transitions occurring at different current values and from one sample to the other. In Fig. 3 we show the temporal evolution of the polarized intensity fluctuations for different transitions of the same laser sample. We can observe that the typical residence times vary from a few tens of ns to a fraction of a second. In other samples, we have observed residence times as long as a few seconds. We remark that the polarized intensity jumps are due, also in these lasers, to transitions between emission configurations where the power is differently distributed between the two polarizations. However, the total power is the same for the two configurations and, as a consequence, the peculiar dynamics is not observed in the total intensity.

The range of Kramers times that characterizes the dynamics of our VCSELs allows us to study SR over unprecedented intervals of time scales. We point out that also for the longer residence times the rise time of the jumps is as short as a few nanoseconds.

Increasing the pump current across the switching region, a transition from a situation where the polarized laser intensity is most of the time in the upper level to one with the intensity mostly in the lower level can be observed. The histograms of the intensity fluctuations change accordingly, namely, from a two-peak shape where the larger peak is on the right to one where it is on the left. In Fig. 4 these histograms are reported

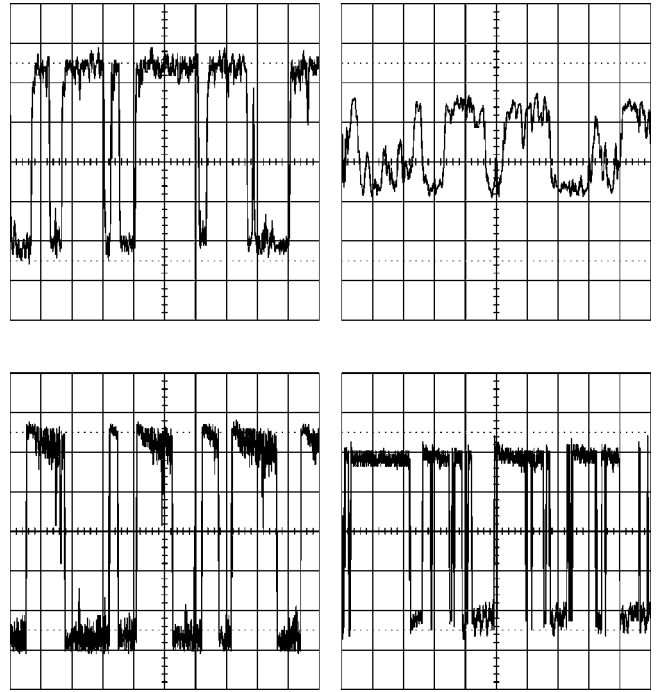


FIG. 3. Time series of the polarized output intensity for different polarization switchings regions in the same laser sample. Horizontal units are, from left to right,  $0.5 \mu\text{s}/\text{div}$  and  $50 \text{ ns}/\text{div}$  (top),  $5 \mu\text{s}/\text{div}$  and  $0.5 \text{ s}/\text{div}$  (bottom).

on a semilogarithmic scale. According to Eq. (2), these probability distributions can be directly interpreted as quasipotentials by simply inverting the vertical axis. Following this interpretation, in the absence of noise-driven jumps the bistable region would correspond to the pump current interval where the quasipotentials display two wells (i.e., two local minima). Increasing the current, the system remains in the upper state while its level corresponds to a local minimum; then it jumps to the lower level and vice versa.

The bistability of the system can be directly shown by sweeping the pump current at a rate much higher than the Kramers time. In this way, the probability of a noise-driven jump is negligible and a plot of the hysteresis loop is obtained (Fig. 5).

It is evident in Fig. 4 that the intensity histograms are in general asymmetric. Their shape depends on the pump current and on the particular transition chosen. This large versatility can be exploited in order to investigate experimentally the peculiar effects on SR due to the shape of the quasipotential (see, for example, [31] for numerical results). This subject is, however, deferred to a further paper; for our work, we have chosen an experimental condition for which

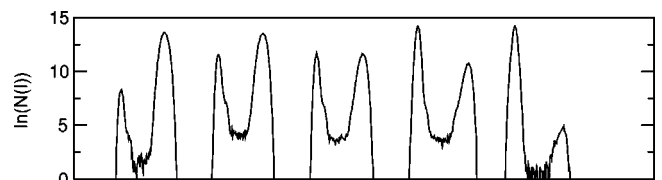


FIG. 4. Histograms  $N(I)$  of the polarized laser intensity  $I(t)$  for different pump currents (increasing from left to right) across the transition investigated through the present work.

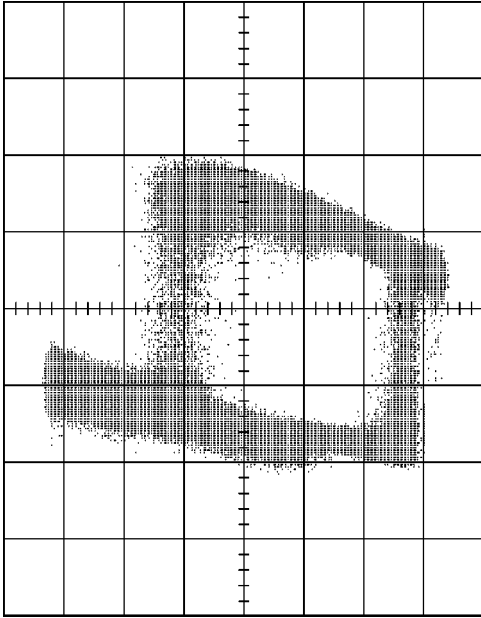


FIG. 5. Hysteresis cycle of the polarized intensity  $I(t)$ . In the abscissa we report the input modulation signal, while the output laser intensity is plotted in the ordinate axis. The laser current increases from right to left.

the time statistics shows a rather symmetric probability distribution. This allows for a simpler interpretation of the results and for a significant comparison with the large number of theoretical and numerical works. We remark, however, that such works are in general based on a symmetric quartic potential, while in our case the quasipotential is flatter at the barrier.

In order to observe a SR effect, a white Gaussian noise has been introduced in the pump current. The experimental evidence of SR and its characterization are the most important results of the present work. However, it is useful to rely on the observed behavior to the Langevin model with the quasipotential. In particular, we have checked that Eq. (2) is still valid when some noise is added to the current, and established a relation between the parameter  $D$  of the model and the amount of noise actually added to the laser pump current. According to Eq. (2) the logarithmic probability densities rescaled with  $D$  give a unique shape, except for a normalization additive constant. We have indeed rescaled the logarithmic histograms for different noise strengths, choosing the scaling factor in order to obtain the best possible overlapping with the original curve (without noise added). We show in Fig. 6 that the different curves are rather well superimposed, and the resulting shape can be considered as the phenomenological quasipotential  $V(q)$  in Eqs. (1) and (2). The scaling factor is reported in Fig. 7 versus the mean square amplitude of the noise  $\xi$  added to the input current, measured at the output of the noise generator. A conversion function can be recovered to pass from  $\xi$  to the parameter  $D/\Delta V$  of the model. The result for different transitions is often a linear relation though slight saturation effects are sometimes present. For the transition used in the present work, the conversion function is

$$\frac{D}{\Delta V} = \frac{a\xi^2}{1 + (\xi/b)^2} + c, \quad (4)$$

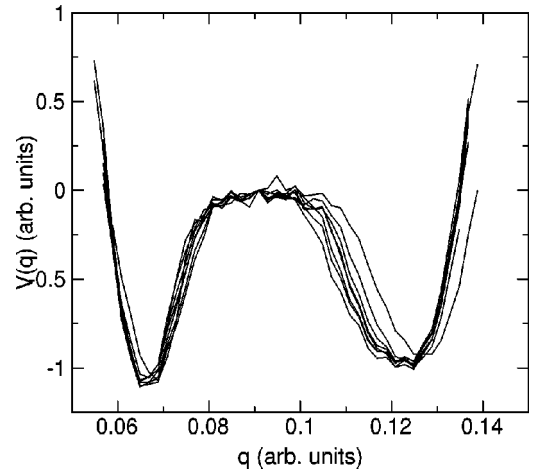


FIG. 6. Quasipotentials deduced from the rescaled experimental intensity histograms.

where  $a = 0.95V^{-2}$ ,  $b = 0.39V$ , and  $c = 9.2 \times 10^{-2}$  are fitting parameters.

The extrapolation to zero input noise ( $\xi = 0$ ) gives somehow the intrinsic noise of the system. We remark that it is not due to the pump current noise, whose effect is negligible, but it is originated by other stochastic phenomena in the laser.

Another important parameter for a quantitative study of SR is the amplitude of the input modulation. In the theoretical model, the temporal evolution is governed by

$$\dot{q} = -\frac{\partial V}{\partial q} + A \cos(\Omega t) + F(t). \quad (5)$$

In our case, the modulation is superimposed to the pump current, and the calibration of  $A$  is obtained from the hysteresis cycle reported in Fig. 5.

Indeed, in the adiabatic approximation and in the presence of modulation, the potential becomes  $V(q, t) = V(q) - qA \cos(\Omega t)$ . In the absence of noise the jumps occur every half modulation period (with a large enough modulation). In the approximation of a quartic symmetric potential, with two wells at  $\pm q_m$  separated by a barrier of height  $\Delta V$ , this happens for

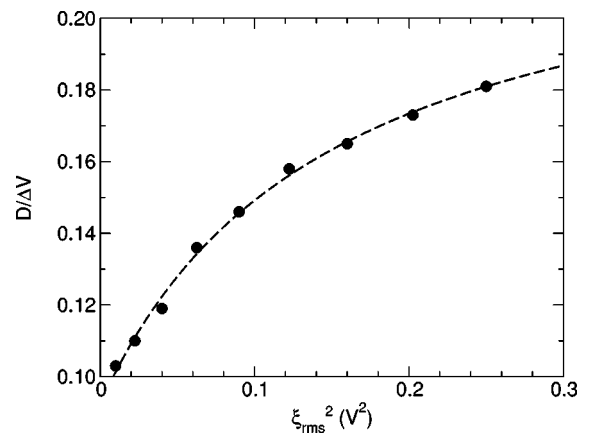


FIG. 7. Normalized noise intensity vs the input noise mean square amplitude. The dashed curve represents a fit with Eq. (4).

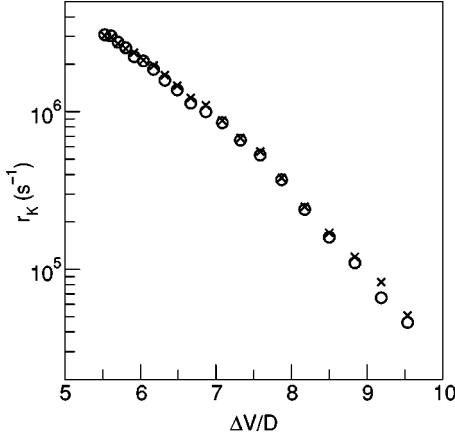


FIG. 8. Kramers rates vs input noise for the upper (crosses) and lower (circles) states.

$$A \cos(\Omega t) = \pm \frac{8}{3\sqrt{3}} \frac{\Delta V}{q_m}$$

(+ stands for jumps from the lower to the upper state and vice versa for the -).

The parameter  $A$ , in terms of  $\Delta V/q_m$ , is thus proportional to the ratio between the amplitude of the modulation superimposed to the laser current and the half-width of the hysteresis cycle. For the transition used in this investigation, this leads to

$$\frac{A q_m}{\Delta V} \approx 1.45 A_{sig}(V), \quad (6)$$

where the  $A_{sig}$  is the signal amplitude measured at the output of the generator.

We have in this way obtained a complete set of conversion functions from the parameters of the experiment to the ones of the model; a quantitative comparison is thus possible.

A further issue in the analysis of the system, before introducing the modulation and studying the features of SR, concerns the statistics of the residence times in the two states. In Fig. 8 we report the Kramers rates deduced from the histograms of the residence times, for both the upper and lower levels. For low noise levels ( $\Delta V/D \gg 1$ ) the Kramers rate  $r_K$ , which is the inverse of the Kramers time  $T_K$ , is expected to be an exponentially decreasing function of the ratio  $\Delta V/D$  [24]. This is what we actually find in our experiment.

#### IV. TEMPORAL AND SPECTRAL ANALYSIS

As expected, a weak modulation of the laser input current produces a slightly modulated intensity which is observed together with rare random jumps between the two levels (Fig. 9). Increasing the amount of noise added to the pump current, the jumps between the two states tend to synchronize with the applied modulation. In this case, the output modulation is much stronger than without input noise. Increasing further the noise, the synchronization is lost due to frequent jumps, yielding quite a noisy output. This is the typical signature of stochastic resonance.

For a more quantitative analysis, the response of the sys-

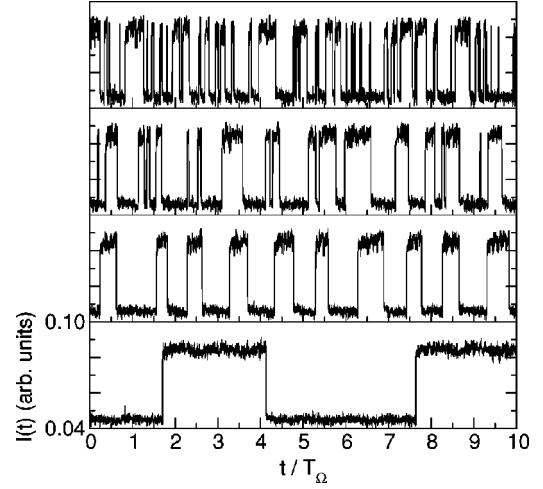


FIG. 9. Time series of the polarized output intensity  $I(t)$  for various noise intensities (increasing from bottom to top:  $D/\Delta V = 0.120, 0.148, 0.165, 0.181$ ) and for a modulation frequency  $\Omega/2\pi = 200$  kHz.

tem to an input modulation at frequency  $\Omega/2\pi$  can be described as a variation of the polarized output intensity  $q$  of the kind  $q(t) = q_0 \cos(\Omega t + \phi)$ . In Fig. 10 we report the observed amplitude  $q_0$ , obtained from the component at  $\Omega/2\pi$  of the frequency spectrum of  $q(t)$ , as a function of the noise. The values of  $q_0$  are normalized to half the difference between the two levels; in this way, a square wave would yield an amplitude of  $4/\pi$ , a value effectively approached by the experimental data. Calculations based on the general bistable quartic potential in the framework of the linear response theory predict an amplitude

$$q_0 \propto \frac{1}{D} \frac{r_K}{\sqrt{4r_K^2 + \Omega^2}}. \quad (7)$$

As shown in Fig. 10 the fit of the experimental data with the above expression (straight line) is in fair agreement with the experimental values (circles). In the fitting procedure we use two free parameters, namely, a multiplicative constant and the scaling factor for  $r_K$ .

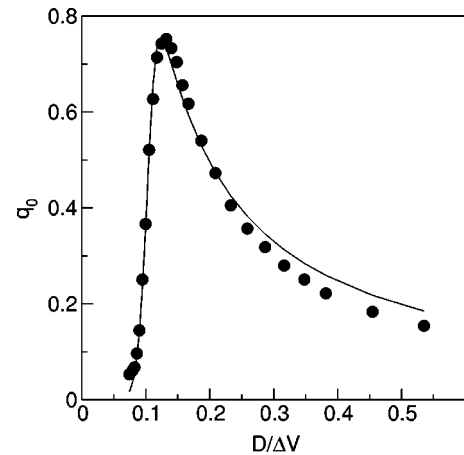


FIG. 10. Amplitude  $q_0$  of the signal vs noise. The predicted value for a perfect synchronization is  $4/\pi$ . The straight line is a fit with Eq. (7). The modulation frequency is 200 kHz.

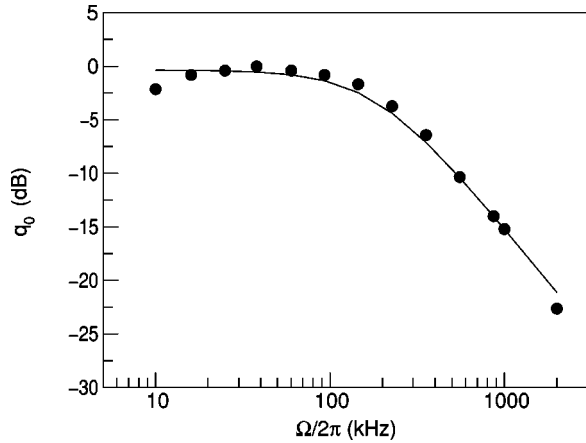


FIG. 11. Frequency response of the signal amplitude  $q_0$  for  $D/\Delta V=0.135$ . The solid line is the fit with a single-pole transfer function, which yields a frequency cutoff at  $\Omega_0/2\pi=180$  kHz.

The physical origin of SR can be found in a time-scale coincidence between the modulation period and the typical time constant (Kramers time) of the system, which monotonically decreases as the noise increases. According to this heuristic argument, one would expect a resonance behavior also by changing the modulation period with fixed noise. On the contrary, calculations based on a simple system (a symmetric, quartic potential) [10] forecast a response characterized only by a single pole at  $\Omega_0=2r_K$ . This prediction was confirmed in our preliminary work [14]. In Fig. 11 the experimental data for  $q_0$  vs  $\Omega$ , with a fixed noise, are reported. The plotted fit gives actually a single-pole behavior, with a cutoff frequency  $\Omega_0/2\pi=180$  kHz. For a more quantitative comparison with theory, we can consider the average residence times in the two levels, measured in the absence of modulation and with the same noise intensity. The measured values are  $T_K^{upper}\simeq T_K^{lower}=1.5\ \mu s$ . The expected cutoff frequency is then  $\Omega_0/2\pi=2/\pi(T_K^{upper}+T_K^{lower})=210$  kHz. The agreement with the measured frequency is good, but further theoretical investigations taking into account the potential shape would certainly be of interest.

## V. STATISTICAL ANALYSIS

The spectral analysis of the output signal was the first tool used to demonstrate the SR effect [1]. A different kind of analysis was later introduced by Gammaitoni *et al.* [32] based on a statistical description of the system behavior in terms of the residence-time probability distribution (RTPD), obtained by monitoring the time spent by the system in each well of the potential. In this way the intrawell motion is neglected and only the jumps between the wells are taken into account. As explained in Sec. III, for the free-running laser the shape of the RTPD is given by a decreasing exponential function. In the presence of a weak modulation with period  $T_\Omega$  and angular frequency  $\Omega=2\pi/T_\Omega$  some peaks appear in the RTPD at approximately  $T_\Omega/2+nT_\Omega$ ,  $n=1,2,\dots$ , superimposed onto the exponential background.

In order to measure the RTPD we acquire, for a given set of parameters, the time series of the polarized intensity with a digital oscilloscope (see Fig. 1). We use a sampling rate of  $10^8$  samples/s and for each acquisition we record  $2\times 10^7$

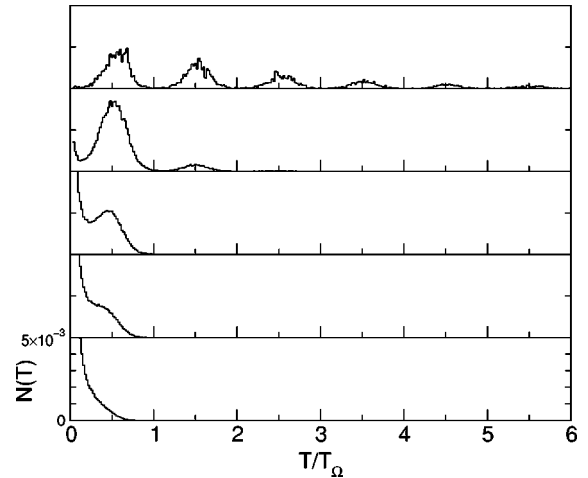


FIG. 12. Residence-time-probability distribution (RTPD) for the upper state for various noise intensities (from top to bottom,  $D/\Delta V=0.104,0.120,0.148,0.157,0.165$ ) and for a modulation frequency  $\Omega/2\pi=1/T_\Omega=200$  kHz.

data points. For this analysis, we use modulation frequencies up to a few hundred kHz. After each acquisition, we compute the RTPD using a simple and fast algorithm transforming the time series into a discrete process, where the ‘‘up’’ and ‘‘down’’ states are defined with respect to a fixed threshold located in correspondence with the potential maximum. All the present results are insensitive to small changes of the threshold level. We define the residence time as the time interval between two successive crossings of the threshold. We note that with this algorithm, an excess of counts can appear for very short events, due to the jitter during the jump.

A typical set of residence time histograms obtained with the above procedure is shown in Fig. 12. For low noise strength, the histogram is composed of several peaks without background, whose amplitudes decrease exponentially. In this situation (see Fig. 9) the amount of noise is not enough to ensure a good synchronization, i.e., a jump from a given well to the other at each multiple of  $T_\Omega/2$ . The system must spend several periods in one well before a jump occurs. For a larger noise strength, the increase of the first peak height can be observed together with the disappearance of higher-order peaks and an increase of the background. This latter component is due to events that are not synchronized with the modulation. When the transition rate between the two wells becomes comparable to twice the modulation frequency, the system is almost fully synchronized and jumps from one state to the other every time the potential barrier is at the minimum, i.e., every  $T_\Omega/2$ . Increasing further the noise strength, the peak structure is destroyed, being hidden behind the background noise.

While some kind of resonant behavior is quite visible following the shape of the RTPDs vs noise, the choice of the indicator for characterizing quantitatively the phenomenon is critical and it is the subject of a recent debate [33,34,14]. A related, important question is whether a resonance in the noise-assisted jumps can be found also as a function of the input signal frequency.

A first indicator was proposed by Gammaitoni *et al.* [33], who monitor the parameter  $P_n$ , defined as the integral of the

RTPD  $N(T)$  over the  $n$ th peak at  $T_n = T_\Omega/2 + nT_\Omega$ ,

$$P_n = \int_{T_n - \alpha T_\Omega}^{T_n + \alpha T_\Omega} N(T) dT, \quad (8)$$

where  $0 < \alpha \leq 1/4$  defines the width of the integration region. The parameter  $\alpha$  seems not to have a major influence on the results. However, it was shown [34] that such an indicator is not appropriate because the amplitude of the background at  $T_n$  exhibits a resonant behavior even in the absence of a periodic driving. To get rid of this problem, Choi *et al.* [34] introduced as a possible indicator of SR the difference between the height of the peak and that of the background at  $T_n$ . They showed that this indicator had a resonancelike behavior as a function of the noise, but a monotonic one as a function of the modulation frequency.

The approach we propose in Ref. [14] is based on a further, slightly different indicator  $\tilde{P}_n$ , i.e., the integral over the  $n$ th peak after the subtraction of the background.

This choice clearly overcomes the criticism of Choi *et al.* and, as we show in the following, presents some advantages with respect to the evaluation of the peak height relative to the background. The indicator  $\tilde{P}_n$  has a deeper physical meaning than the height of the peak. Indeed, the latter indicator leads to results which depend on the width of the bins chosen for the RTPD. Thus, the use of  $\tilde{P}_n$  is not only correct, but even preferable. However, the separation of the peaks from the background needs an accurately checked fitting procedure.

We use two different functions for fitting the experimental RTPDs. A first one is defined as

$$f(T) = a_0 e^{-a_1 T} + \sum_n b_n G(T - (T_0 + nT_\Omega), \sigma), \quad (9)$$

where  $a_0, a_1, b_n, T_0, \sigma$  are fitting parameters and  $G(T, \sigma)$  is a Gaussian centered at  $T=0$  of width  $\sigma$ :

$$G(T, \sigma) = \exp(-T^2/\sigma^2). \quad (10)$$

The second function is

$$g(T) = a_0 \exp[-a_1 T - a_2 \cos(\Omega T + a_3)], \quad (11)$$

with fitting parameters  $a_0, a_1, a_2, a_3$ . For each experimental curve, both functions are used and the results compared. What is found is that the best choice depends on the number of peaks considered in the histogram. If only one or two peaks are visible (case I), the function  $f(T)$  gives a better result, whereas for a large number of peaks (case II) a fit with the function  $g(T)$  is better. The correct estimation of the background depends crucially on the quality of the fit. However, there is a wide region of the input parameters ( $\Omega$  and  $D$ ) where the two expressions give very close fitting curves. An example is shown in Fig. 13, for  $D/\Delta V = 0.135$  and  $\Omega/2\pi = 284$  kHz. Some small discrepancies can be seen in the first bins of the histograms, where an erroneous counting is expected due to the very fast dynamics around the unstable point, increased in our case by the flatness of the potential. Löfstedt and Coppersmith [35,36] found, in the limit of a vanishing modulation amplitude ( $A \rightarrow 0$ ) and small noise (but with  $A/D$  remaining small), an expression for the

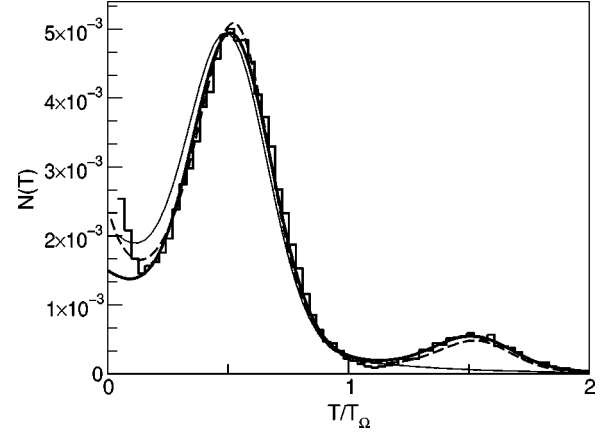


FIG. 13. Comparison between the fits of an experimental RTPD (stepped) with  $f(T)$  (thick solid line) and with  $g(T)$  (long-dashed line). The thin solid line represents the Gaussian approximation of  $g(T)$  around the first peak [Eq. (14)]. See text for the definition of fitting functions.

RTPD close to  $g(T)$ , i.e., a decreasing exponential multiplied by a sine function. Our parameters are, however, in a range where analytical expressions can hardly be applied ( $Aq_m/\Delta V \approx 0.26$ ,  $Aq_m/D \approx 1$ ).

In the two cases the indicator  $\tilde{P}_n$  is defined as

$$\tilde{P}_n = \int_{-\infty}^{\infty} G(T - (T_0 + nT_\Omega), \sigma) dT \quad (12)$$

and

$$\tilde{P}_n = \int_{\theta_1}^{\theta_2} [g(T) - a_0 \exp(-a_1 T - a_2)] dT \quad (13)$$

where  $\Omega\theta_1 + a_3 = 2\pi n$  and  $\Omega\theta_2 + a_3 = 2\pi(n+1)$ .

Moreover, in order to draw a closer link between the two expressions we point out that  $g(T)$  can be approximated around the first peak by the sum of an exponential and a Gaussian:

$$g(T) \approx \alpha \exp(-(T - T_0)^2/\sigma^2) + \beta \exp(-a_1 T), \quad (14)$$

where  $\alpha = 2a_0 e^{-a_1 T_0} \sinh(a_2 \cos a_3)$ ,  $\sigma^2 = 2/a_2 \Omega^2 \cos a_3$ , and  $\beta = a_0 e^{-a_2}$ .

In Fig. 14 are plotted  $\tilde{P}_n$  versus  $D/\Delta V$  for  $Aq_m/\Delta V = 0.26$  and  $\Omega/2\pi = 200$  kHz for both the lower and upper states.

Our work presents an experimental investigation of SR in terms of RTPDs. The trend of the first peak intensity  $\tilde{P}_0$ , with evidence of resonant behavior, has already been reported in our previous work [14], whereas here we extend the analysis to the higher-order peaks.

Until now investigation of the trend of the peaks intensity, for the different order  $n$ , has been carried out by means of analog simulations and approximated analytic calculations [33,10]. The high quality of our signals and the huge amount of data we can accumulate, thanks to the stability of the system, allow a complete comparison with theoretical forecasts. We stress that, with respect to the usual theoretical

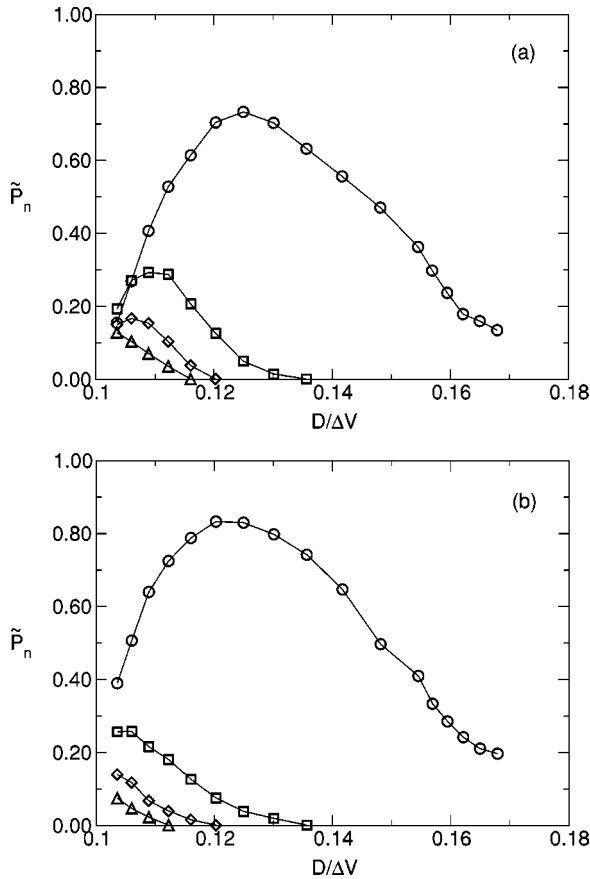


FIG. 14. Indicator  $\tilde{P}_n$  for the lower (a) and the upper (b) states for a constant modulation frequency  $\Omega/2\pi=200$  kHz versus the input noise. The curves refer to the first (circles), second (squares), third (diamonds), and fourth (triangles) peaks in the RTPDs. Solid lines are to guide the eye.

calculations, we use slightly different indicators. The effect of this choice is to be evaluated and should be particularly evident for high noise levels.

The main topics of the RTPD analysis are summarized in [10] as follows.

(a) For low  $D$  levels, all the  $\tilde{P}_n$  should tend to a constant value [33]. This effect can be guessed from the plot in Fig. 14. This is related to the fact that, as already noticed, for low noise the intensity of the peaks shows an exponentially decreasing trend, with a larger decay constant corresponding to lower  $D$ .

(b) While the resonance is more clearly evident for  $\tilde{P}_0$ , also the higher-order peaks should exhibit a resonant behavior, in correspondence with decreasing input noise level. More precisely, the Kramers rates corresponding to the abscissa of the maxima should satisfy

$$(2n+1)r_K \approx 2/T_\Omega. \quad (15)$$

This feature is confirmed by our data, in particular by the RTPD corresponding to the lower state [Fig. 14(a)].

(c) The resonance should occur at a lower noise level for  $\tilde{P}_0$  than for the amplitude of the output signal  $q_0$  [33]. In particular,  $\tilde{P}_0$  should reach its maximum when  $r_K \approx 2/T_\Omega$ ,

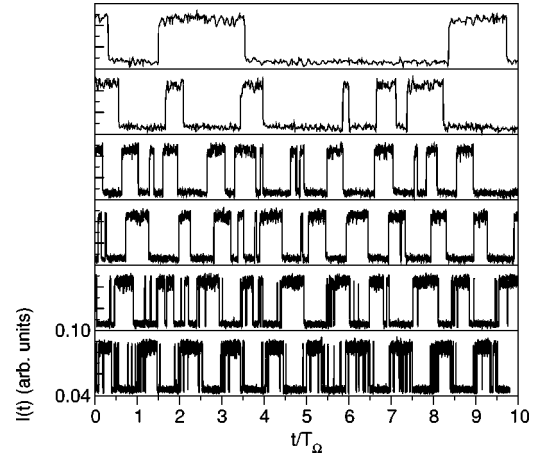


FIG. 15. Time series of the polarized output intensity  $I(t)$  for  $D/\Delta V=0.158$  and for increasing modulation frequency. From bottom to top 20,40,120,160,640,1200 kHz. The horizontal axis is always ten modulation periods long.

according to Eq. (15). In our case, the maximum of  $\tilde{P}_0$  is around  $D/\Delta V \approx 0.125$ . This is in good agreement with the value  $D/\Delta V \approx 0.13$  inferred from Fig. 8, in correspondence with a rate  $r_K = 4 \times 10^5 \text{ s}^{-1}$ . The maximum of  $q_0$  is instead found at  $D/\Delta V \approx 0.14$ .

Since the potential is not strictly symmetric, the curves for the indicators are different in the two states [Figs. 14(a), and 14(b)]. This effect cannot be revealed with a frequency analysis of the response (Fig. 10), and allows to one get some more information on the potential. A more detailed investigation about the consequences of an asymmetric potential would be interesting and will be carried out in future works.

A complementary investigation can also be performed, namely, the examination of the RTPDs when changing the frequency of the input signal for a fixed amount of noise. As shown above (see Fig. 11), in such a case the output signal shows a single pole behavior in the frequency domain. How-

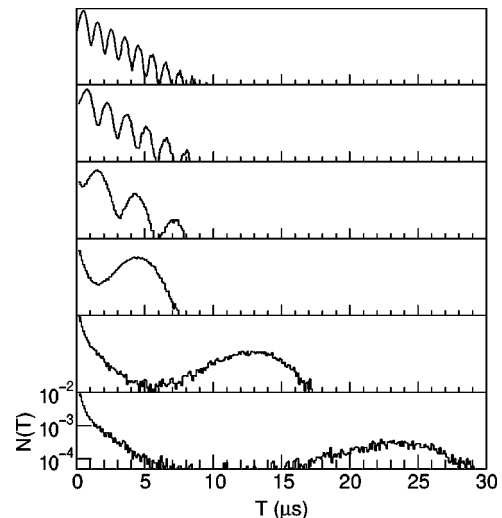


FIG. 16. Logarithm of the RTPD for  $D/\Delta V=0.135$  for the upper state. From bottom to top the modulation frequency reads 20,38,116,355,694,1000 kHz.

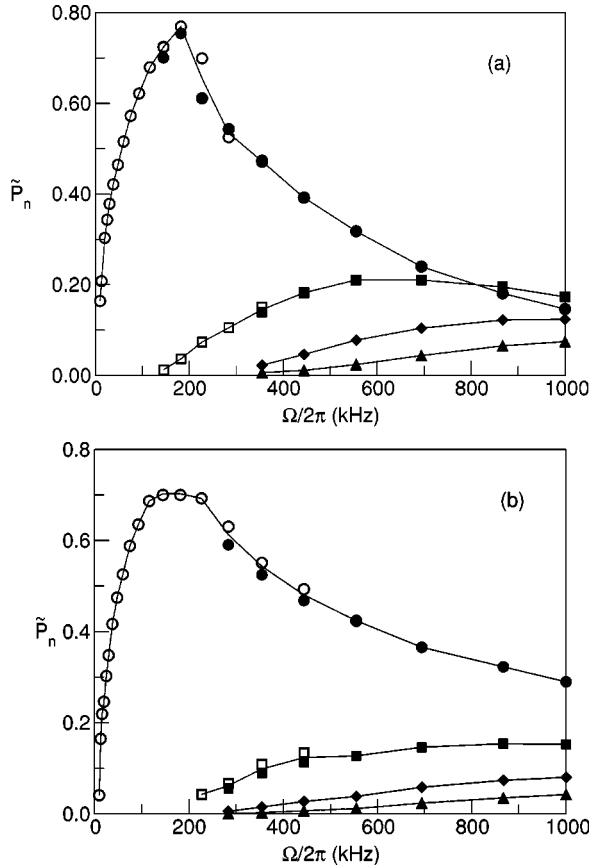


FIG. 17. Indicator  $\tilde{P}_n$  for the lower (a) and the upper (b) states vs the modulation frequency for a constant input noise  $D/\Delta V = 0.135$ . The curves refer to the first (circles), second (squares), third (diamonds), and fourth (triangles) peaks in the RTPDs. Open symbols are results obtained with the fitting function  $f(T)$ , while solid symbols refer to function  $g(T)$ . Solid lines are to guide the eye.

ever, a plot of the time series (Fig. 15) reveals that there exists a modulation frequency for which the output signal appears “regular,” i.e., mostly synchronized with the input signal. Indeed, for low modulation frequencies, it is quite likely that the system performs random jumps (with the Kramers rate) during the modulation period. On the contrary, at high frequencies, the system cannot follow completely the modulation and often remains in the same state during several periods. In the intermediate situation, i.e., for a frequency around  $r_K/2$ , a time-scale coincidence between random jumps and modulation leads to a synchronization of the output.

The RTPDs (see Fig. 16) exhibit an exponentially decreasing background, with a superimposed regular structure of peaks. Above all for high frequencies, the fit of the histograms must be carefully performed, in order to clearly separate the background. The resulting indicators  $\tilde{P}_n$  are reported in Fig. 17. For the region  $180 \text{ kHz} \leq \Omega/2\pi \leq 550 \text{ kHz}$ , we plot the results obtained for both above-defined fitting expressions, showing good agreement and a smooth transition between the two methods. While  $q_0$  is almost constant (until the cutoff frequency is approached), the indicator  $\tilde{P}_0$  clearly shows a resonance.

Such a phenomenon was introduced by [33] and called *bona fide* resonance. Experimental evidence is given in our

previous work [14]. Even if the prediction of a system resonance vs frequency given in Ref. [33] is based on an incorrect indicator, as pointed out by Choi *et al.* [34], our results demonstrate that the phenomenon is effective, at variance with what asserted in Ref. [34]. The disagreement with this last work comes from the different choice of indicator: as experimentally confirmed in our previous work [14], their peak-to-background quantifier yields a monotonous function of  $\Omega$ .

The physical reason why for low frequencies the peak intensity decreases yielding the resonance, differently from  $q_0$ , is the following. The occurrence of some short random jumps superimposed onto the synchronized, square-wave response (see Fig. 15, bottom) lowers significantly the probability to have a residence time of  $T_\Omega/2$ . On the other hand, it does not substantially decrease the spectral power at  $\Omega$ .

As for the resonance versus noise, also the indicator for the higher-order peak  $\tilde{P}_1$  shows a maximum. The abscissas of the maxima are in good agreement with the rule  $\Omega_n/2\pi = (2n+1)r_K/2$  [see Eq. (15)].

## VI. CONCLUSIONS

We report a detailed experimental analysis of SR in VCSELs.

We show how, for a particular value of the pump current, the laser is bistable and the polarized intensity is characterized by noise-induced jumps between two levels, with a Kramers statistics. A suitable Langevin model of the local dynamics is carried out, giving a correct description of the statistics of the jumps.

The application of an external modulation and a white, Gaussian noise on the pump current allows the observation of SR, i.e., the noise-induced enhancement of the output signal.

The calibration of the experimental parameters in terms of the model variables is performed, thus allowing a complete comparison with the existing theories.

The SR is studied both in the temporal and in the frequency domain. Moreover, the statistical analysis in terms of RTPDs, used in an experimental work in [14], is here extended and detailed.

The phenomenon of SR was until now widely characterized by theoretical calculations and numerical and analog simulations. Our work opens the way to a completely new kind of study, dealing with a real physical system. Indeed, with respect to previous experimental observations, our apparatus allows one to accurately control the parameters over a large range and to perform exhaustive statistical analyses thanks to the huge amount of data that can be acquired. The features of our system permit one to effectively test the validity of theoretical calculations and stimulate further investigations.

## ACKNOWLEDGMENTS

We acknowledge partial support from Contract No. 96.00267.CT02 of the Italian National Council of Research (CNR). S.B. acknowledges EU support through TMR grant “Marie-Curie” No. ERBFMBICT983351. We thank Ivan Rabbiosi for the help provided during the initial stage of this work.

- [1] R. Benzi, A. Sutera, and A. Vulpiani, *J. Phys. A* **14**, 453 (1981).
- [2] R. Benzi, G. Parisi, A. Sutera, and A. Vulpiani, *Tellus* **34**, 10 (1982).
- [3] C. Nicolis and G. Nicolis, *Tellus* **33**, 225 (1981).
- [4] S. Fauve and F. Heslot, *Phys. Lett.* **97A**, 5 (1983).
- [5] B. McNamara, K. Wiesenfeld, and R. Roy, *Phys. Rev. Lett.* **60**, 2626 (1988).
- [6] B. McNamara and K. Wiesenfeld, *Phys. Rev. A* **39**, 4854 (1989).
- [7] F. Marchesoni, E. Menichella-Saetta, M. Pochini, and S. Santucci, *Phys. Rev. A* **37**, 3058 (1988).
- [8] T. Zhou and F. Moss, *Phys. Rev. A* **41**, 4255 (1990).
- [9] T. Zhou, F. Moss, and P. Jung, *Phys. Rev. A* **42**, 3161 (1990).
- [10] L. Gammaitoni, P. Hänggi, P. Jung, and F. Marchesoni, *Rev. Mod. Phys.* **70**, 223 (1998).
- [11] F. Noss, A. Bulsara, and M. Shlesinger, *Proceedings of the NATO Advanced Research Workshop on Stochastic Resonance in Physics and Biology*, edited by F. Moss, A. Bulsara, and M. F. Shlesinger [*J. Stat. Phys.* **70**, No. 1/2 (1993)].
- [12] A. Fioretti, L. Guidoni, R. Mannella, and E. Arimondo, *J. Stat. Phys.* **70**, 403 (1993).
- [13] J. M. Iannelli, A. Yariv, T. R. Chen, and Y. H. Zhuang, *Appl. Phys. Lett.* **65**, 1983 (1994).
- [14] G. Giacomelli, F. Marin, and I. Rabbiosi, *Phys. Rev. Lett.* **82**, 675 (1999).
- [15] M. P. van Exter, A. Al-Remawi, and J. Woerdman, *Phys. Rev. Lett.* **80**, 4875 (1998).
- [16] K. Choquette, D. Ritchie, and R. Leibenguth, *Appl. Phys. Lett.* **64**, 2062 (1994).
- [17] J. Epler *et al.*, *Appl. Phys. Lett.* **69**, 722 (1996).
- [18] G. Giacomelli *et al.* *Opt. Commun.* **146**, 136 (1998).
- [19] G. Giacomelli and F. Marin, *Quantum Semiclassic. Opt.* **10**, 469 (1998).
- [20] J. van't Hoff, *Etudes de Dynamiques Chimiques* (Muller, Amsterdam, 1884).
- [21] S. Arrhenius, *Z. Phys. Chem. (Leipzig)* **4**, 226 (1889).
- [22] P. Artusi, *La Scienza in Cucina e l'Arte di Mangiar Bene* (Landi, Firenze, 1891).
- [23] H. Kramers, *Physica (Utrecht)* **7**, 284 (1940).
- [24] P. Hänggi, P. Talkner, and M. Borkovec, *Rev. Mod. Phys.* **62**, 251 (1990).
- [25] N. G. van Kampen, *Stochastic Processes in Physics and Chemistry* (Elsevier, Amsterdam, 1997).
- [26] F. Marin and G. Giacomelli, *J. Opt. Soc. Am. B* **1**, 128 (1999).
- [27] M. SanMiguel, Q. Feng, and J. V. Moloney, *Phys. Rev. A* **52**, 1728 (1995).
- [28] F. Prati, G. Giacomelli, and F. Marin (unpublished).
- [29] M. S. Miguel, in *50th Scottish Universities Summer School in Physics, Semiconductor Quantum Optoelectronics*, edited by A. Miller (Elsevier, Amsterdam, 1999).
- [30] M. P. van Exter, M. B. Willemsen, and J. P. Woerdman, *Phys. Rev. A* **58**, 4191 (1998).
- [31] A. R. Bulsara, M. E. Inchiosa, and L. Gammaitoni, *Phys. Rev. Lett.* **77**, 2162 (1996).
- [32] L. Gammaitoni, F. Marchesoni, E. Menichella-Saetta, and S. Santucci, *Phys. Rev. Lett.* **62**, 349 (1989).
- [33] L. Gammaitoni, F. Marchesoni, and S. Santucci, *Phys. Rev. Lett.* **74**, 1052 (1995).
- [34] M. H. Choi, R. F. Fox, and P. Jung, *Phys. Rev. E* **57**, 6335 (1998).
- [35] R. Löfstedt and S. N. Coppersmith, *Phys. Rev. Lett.* **72**, 1947 (1994).
- [36] R. Löfstedt and S. N. Coppersmith, *Phys. Rev. E* **49**, 4821 (1994).